Chapter 4

Magnetised CMBR anisotropies in a reionised scenario

[1]This chapter is based the paper: Gopal & Sethi, 2005, Phys.Rev.D.

Summary and the main results of chapter 4

A primordial magnetic field sources all the three types of perturbations in the plasma i.e scalar corresponding to density perturbations, vector corresponding to vorticity perturbations and tensor corresponding to gravitational waves. Each of these perturbations will produce its specific signature in the CMBR anisotropies and hence a detailed study of such effects can be done to either detect or constrain the magnetic field. In this chapter we work out in a semi-analytic manner the contribution to the temperature as well as the polarization anisotropies of CMBR in the reionised scenario. In particular we found that the most interesting signal on large scales which reflects in the CMBR at low multipoles comes from tensor perturbations. We also investigated the possibility that an equal combination of both magnetic field sourced tensor mode and primordial scalar modes contributes to the net angular power spectrum on large scales. In addition to the above, we also evaluate the contributions of magnetised vector and scalar modes to the CMBR anisotropies

The main results are summarized below:

- ***The temperature-polarization cross correlation due to magnetised tensor perturbation can explain the observed enhancement in the corresponding signal in the recent WMAP data for a nearly scale-invariant spectrum of the magnetic field of strength*** 4.5 ***nano-gauss.***

- ***In the scenario in which an equal combination of both magnetic field sourced tensor mode and primordial scalar modes contributes to the net angular power spectrum on large scales, we find that the current bounds on the optical depth to reionisation of 0.17, which is deduced from the WMAP data assuming contribution from primordial scalar modes only, can be reduced to about 0.11.***

- ***The magnetised vector mode contribution to CMBR anisotropies produces observable effects at very small scales which will be probed in future experiments like PLANCK whereas scalar modes in general produce very weak signals.***

4.1 Introduction

In the first chapter we worked out the observable consequences of large-scale magnetic fields on the clustering properties of matter at the current epoch. In particular, we studied quantitatively the manner in which the existence of primordial magnetic fields of nano-Gauss strength can influence the large scale structure formation in the Universe (Wasserman 1978, Kim, Olinto & Rosner 1996, Subramanian & Barrow 1998, Sethi 2003, Gopal & Sethi 2003, Sethi & Subramanian 2005). Another important complementary probe of large-scale fluctuations in the early Universe is the cosmic microwave background radiation (CMBR). The presence of magnetic fields could leave observable signatures in the CMBR anisotropies by having a dynamical effect on the ionised plasma. (Barrow et al. 1997, Subramanian & Barrow 1998, Subramanian & Barrow 2002, Durrer, Ferreira & Kahniashvili 2000, Seshadri & Subramanian 2001, Mack et al. 2002, Lewis 2004).

In recent years, the study of CMBR anisotropies has proved to be the best probe of the theories of structure formation in the universe (see e.g. Hu & Dodelson (2002) for a recent review). The simplest model of scalar, adiabatic perturbations, generated during the inflationary era, appear to be in good agreement with both the CMBR anisotropy measurements and the distribution of matter at the present epoch (see e.g. Spergel 2003, Tegmark et al. 2004). In addition to scalar perturbations, there also exists the possibility of the presence of tensor perturbations to the metric. Tensor perturbations could have been sourced by primordial gravitational waves during the inflationary epoch. There is no definitive evidence of the existence of tensor perturbations in the CMBR anisotropy data; the WMAP experiment, from temperature anisotropy data, obtained upper limits on the amplitude of tensor perturbations (Spergel 2003). Vector perturbations are generally not considered in the standard analysis as the primordial vector perturbations would have decayed by the epoch of recombination in the absence of a continual source. In such a case, these perturbations may not be important in contributing to an observable effect on the large-scale matter distribution. An indisputable signal of vector and tensor modes is that unlike scalar modes these perturbations generate *B*-type CMBR polarization anisotropies (see e.g. Hu & White 1997 and references therein). At present, only upper limits exist on this polarization mode (Kovac et al. 2002). However, the on-going CMBR probe WMAP and the upcoming experiment PLANCK have the capability of unravelling the effects of vector and tensor perturbations.

Recent WMAP results suggest that the universe underwent a transition from being mostly neutral to being predominantly ionised at the epoch of re-ionization at $z \simeq 15$; in particular WMAP analysis concluded that the optical depth to the last reionization surface is $\tau_{\rm reion} = 0.17 \pm 0.04$ (Kogut et al. 2003); which means that nearly 20% of CMBR photons re-scattered during the period of reionization. The secondary anisotropies generated during

this re-scattering leave interesting signatures especially in CMBR polarization anisotropies (see e.g. Zaldarriaga 1997), as is evidenced by the recent WMAP results (Kogut et al. 2003).

Primordial magnetic fields source all the three kinds of perturbations viz. scalar corresponding to density perturbations, vector corresponding to vorticity and tensor corresponding to gravitational waves. Each of these perturbations affect the photon-baryon plasma on different scales and hence produce distinct signals in the CMBR anisotropy spectrum. Different aspects of this problem have been studied earlier by various authors for the scenario of standard recombination history (Giovannini 2005 and references therein). The presence of a second scattering surface (i.e the reionisation surface) in addition to the recombination scattering surface however can lead to additional features in the observed net anisotropy. These features are referred to as secondary CMBR anisotropies.

In this chapter we study the secondary CMBR anisotropies, generated during the epoch of reionization, from vector, tensor, and scalar modes, in the presence of primordial tangled magnetic fields. Recently, Lewis (2004) computed fully-numerically CMBR vector and tensor temperature and polarization anisotropies in the presence of magnetic fields including the effects of reionization. Seshadri & Subramanian (2005) calculated the secondary temperature anisotropies from vector modes owing to reionization. Our approach is to compute the secondary temperature and polarization anisotropies semi-analytically by identifying the main sources of anisotropies in each case; we compute the anisotropies by using the formalism of Hu & White (1997). We also compute the tensor primary signal to compare with the already existing analytical results for tensor anisotropies (Mack et al. 2002) .

In the next section, we set up the preliminaries by discussing the models for primordial magnetic fields and the process of reionization. In §3, §4, and §5, we consider vector, tensor, and scalar modes. In §6 the detectability of the signal is discussed. In §7, we present and summarize our conclusions. While presenting numerical results in this chapter, we use the currently-favoured FRW model: spatially flat with $\Omega_m = 0.3$ and $\Omega_\Lambda = 0.7$ (Spergel 2003, Perlmutter et al. 1999, Riess et al. 2004) with $\Omega_b h^2 = 0.024$ (Spergel 2003, Tytler et al. 2000) and $h = 0.7$ (Freedman et al. 2001).

4.2 Primordial magnetic fields, reionization, and CMBR anisotropies

Assuming that the tangled magnetic fields are generated by some process in the early universe, e.g. during inflationary epoch, magnetic fields at large scales ($\gtrsim 0.1\,\mathrm{Mpc}$) are not affected appreciably by different processes in either the pre-recombination or the post-recombination universe (Sethi & Subramanian 2005, Jedamzik et al. 1998 , Subramanian & Barrow 1998). In this regime, the magnetic field decays as $1/a^2$ from the expansion of

the universe. This allows us to express: $\mathbf{B}(\mathbf{x},\eta) = \tilde{\mathbf{B}}(\mathbf{x})/a^2$; here $\mathbf{x}$ is the comoving coordinate. We further assume tangled magnetic fields, $\tilde{\mathbf{B}}$, present in the early universe, to be an isotropic, homogeneous, and Gaussian random process. This allows one to write, in Fourier space (see .e.g. Landau & Lifshitz 1987):

$$\langle \tilde{B}_i(\mathbf{q})\tilde{B}^*_j(\mathbf{k})\rangle = \delta^3_D(\mathbf{q}-\mathbf{k})\left(\delta_{ij} - k_i k_j/k^2\right) M(k) \tag{4.1}$$

Here $M(k)$ is the magnetic field power spectrum and $k = |\mathbf{k}|$ is the comoving wavenumber. We assume a power-law magnetic field power spectrum here: $M(k) = Ak^n$. We consider the range of scales between $k_{\rm min}$ taken to be zero here and small scale cut-off at $k = k_{\rm max}$; $k_{\rm max}$ is determined by the effects of damping by radiative viscosity before recombination. Following Jedamzik et al. (1998), $k_{\rm max} \simeq 60\,{\rm Mpc}^{-1}(B_0/(3\times10^{-9}\,{\rm G})$; B_0 is the RMS of magnetic field fluctuations at the present epoch. A can be calculated by fixing the value of the RMS of the magnetic field, B_0, smoothed at a given scale, $k_{\rm c}$. Using a sharp k-space filter, we get,

$$A = \frac{\pi^2(3+n)}{k_c^{(3+n)}} B_0^2 \tag{4.2}$$

We take $k_c = 1{\rm Mpc}^{-1}$ throughout this chapter. For $n \simeq -3$, the spectral indices of interest in this chapter, the RMS filtered at any scale has weak dependence on the scale of filtering.

Recent WMAP observations showed that the universe might have got ionized at redshifts $z \simeq 15$. However the details of the ionization history of the universe during the reionization era are still unknown; for instance the universe might have got reionized at $z = 15$ and remained fully ionized till the present or the universe might have got partially reionized with ionized fraction $x_e \lesssim 0.3$ at $z \simeq 30$ and became fully ionized for $z \lesssim 10$. Both these ionization histories are compatible with the WMAP results (Kogut et al. 2003). Given this lack of knowledge we model the reionization history by assuming the following visibility function, which gives the normalized probability that the photon last scattered between epoch η and $\eta + d\eta$, to model the period of reionization:

$$g(\eta,\eta_0) \equiv \dot{\tau}\exp(-\tau) = \frac{(1-\exp(-\tau_{\rm reion}))}{\sqrt{\pi}\Delta\eta_{\rm reion}} \exp\left[-(\eta-\eta_{\rm reion})^2/\Delta\eta^2_{\rm reion}\right] \tag{4.3}$$

Here $\tau(\eta,\eta_0) = \int_{\eta_0}^{\eta} n_e\sigma_t dt$ is the optical depth from Thompson scattering; $\tau_{\rm reion}$ is the optical depth to the epoch of reionization; for compatibility with WMAP results, we use $\tau_{\rm reion} = 0.17$ throughout. $\eta_{\rm reion}$ and $\Delta\eta_{\rm reion}$ are the epoch of reionization and the width of reionization phase, respectively; we take $\eta_{\rm reion}$ corresponding to $z_{\rm reion} = 15$ and $\Delta\eta_{\rm reion} = 0.25\eta_{\rm reion}$. Notice that the visibility function is normalized to $\tau_{\rm reion}$ for $\tau_{\rm reion} << 1$.

4.3 CMBR anisotropies from vector modes

From a given wave number k of vector perturbations, the contribution to CMBR temperature and polarization anisotropies to a given angular mode ℓ can be expressed as (see e.g. Hu &

White 1997):

$$\frac{\Theta^{\rm v}_{T\ell}(\eta_0,k)}{(2\ell+1)} = \int_0^{\eta_0} d\eta\, \exp(-\tau)\left[\dot\tau(v^{\rm v}_{\rm b}-V)\,j^{(11)}_\ell[k(\eta_0-\eta)] + (\dot\tau P^{\rm v}(\eta)+\frac{1}{\sqrt{3}}kV)\,j^{(21)}_\ell[k(\eta_o-\eta)]\right] \quad (4.4)$$

$$\frac{\Theta^{\rm v}_{E\ell}(\eta_0,k)}{(2\ell+1)} = -\sqrt{6}\int_0^{\eta_0} d\eta\, \exp(-\tau)\dot\tau P^{\rm v}(\eta)\epsilon^{\rm v}_\ell[k(\eta_0-\eta)] \quad (4.5)$$

$$\frac{\Theta^{\rm v}_{B\ell}(\eta_0,k)}{(2\ell+1)} = -\sqrt{6}\int_0^{\eta_0} d\eta\, \exp(-\tau)\dot\tau P^{\rm v}(\eta)\beta^{\rm v}_\ell[k(\eta_0-\eta)] \quad (4.6)$$

Here $v^{\rm v}_{\rm b}$ and V are the line-of-sight components of the vortical component of the baryon velocity and the vector metric perturbation. $P^{\rm v}(\eta) = 1/10[\Theta^{\rm v}_{T2} - \sqrt{6}\Theta^{\rm v}_{E2}]$ and the Bessel functions, j_ℓ, ϵ_ℓ and β_ℓ that give radial projection for a given mode are given in Hu & White (1997). The evolution of vector metric perturbations, $V_i(\mathbf{k},\eta)$ is determined from Einstein's equations (e.g. Hu & White 1997, Mack et al. 2002):

$$\dot V_i + 2\frac{\dot a}{a}V_i = -\frac{16\pi G a^2 S_i(\mathbf{k},\eta)}{k} \quad (4.7)$$

$$-k^2 V_i = 16\pi G a^2 \sum_j (\rho_j + p_j)(v^{\rm v}_{ij} - V_i) \quad (4.8)$$

Here S_i, the source of vector perturbations, is determined by primordial tangled magnetic field in our analysis. The index j corresponds to baryonic, photons and dark matter vortical component of velocities. For tangled magnetic fields, the vortical velocity component of the dark matter does not couple to the source of vector perturbations to linear order and $\Omega_i = v^{\rm v}_i - V_i$ decays as $1/a$ for dark matter (see e.g. Mack et al. 2002); and hence the dark matter contribution can be dropped from the Einstein's equations. The photons couple to baryons through Thompson scattering. In the pre-recombination epoch, the photons are tightly coupled to the baryons as the time scale of Thompson scattering is short as compared to the expansion rate; besides the photon density is comparable to baryon density at the epoch of recombination. In the reionized models we consider here, neither the photons are tightly coupled to baryons nor are they dynamically important. Therefore photon contribution can also be neglected in Eq. (4.8). Eq. (4.8) then simplifies to:

$$-k^2 V_i = 16\pi G a^2 \rho_B \Omega^{\rm v}_B \quad (4.9)$$

with $\Omega^{\rm v}_B = (v^{\rm v}_{\rm b} - V_i)$. The quantity of interest is the angular power spectrum of the CMBR anisotropies which is obtained from squaring Eqs. (4.4), (4.5), and (4.6), taking ensemble average, and integrating over all k:

$$C_{\ell T,E,B} = \frac{4}{\pi}\int dk k^2 \left[\frac{\Theta_{T,E,B\ell}(k,\eta_0)}{2\ell+1}\right]^2 \quad (4.10)$$

This expression is valid for both vector and tensor perturbations; for scalar perturbation the prefactor is $2/\pi$.

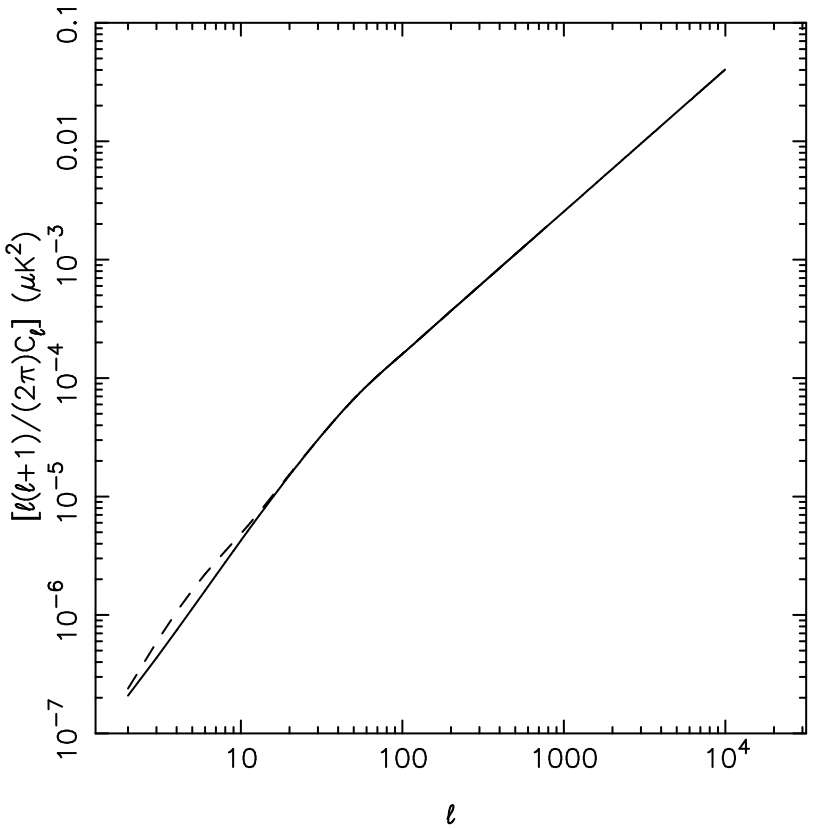

Figure 4.1: The secondary temperature angular power spectrum from vector modes is shown. The solid and the dashed lines correspond to the contribution from vorticity and the total signal, respectively (see text for details). The power spectrum is plotted for $B_0 = 3 \times 10^{-9}$ and $n = -2.9$ (Eq. (4.2)).

For primordial magnetic field, the sources $S_i(\mathbf{k}, \eta)$ of vector perturbation (Eq. (4.7)) is the vortical component of the Lorentz force:

$$S_i(\mathbf{k}, \eta) = \frac{1}{a^4 4\pi} \hat{k} \mathrm{x} \mathrm{F.T.}[\tilde{\mathbf{B}}(\mathbf{x}) \mathrm{x} (\nabla \mathrm{x} \tilde{\mathbf{B}}(\mathbf{x}))] \equiv S_i(\mathbf{k}) \frac{1}{a^4} \tag{4.11}$$

It can be checked that this Newtonian expression for S_i is the same as the more rigorously defined Π_i^V in Appendix A (Eq. (4.28)).

4.3.1 Temperature anisotropies from vector modes

As seen from Eq. (4.4), there are three sources of temperature anisotropies. The most important contribution comes from vorticity Ω_B^{v}. For the reionized models, using Eqs. (4.7) and (4.8), it can be expressed as:

$$\Omega_B^{\mathrm{v}}(\mathbf{k}, \eta) = \frac{k S_i(\mathbf{k}) \eta}{a \rho_{b0}} \tag{4.12}$$

Here ρ_{b0} is the baryon density at the present epoch. The other major contribution is from temperature quadrupole Θ_{T2}^{v}. For reionized models, the quadrupole at the epoch of reion-

ization is dominated by the free-streaming of the dipole from the last scattering surface (see discussion below, Eq. (4.15)). This contribution is generally small but in this case can be comparable to the vorticity effects at small values of ℓ. This is owing to the fact that the vorticity is decaying and therefore during reionization epoch its contribution is smaller as compared to the epoch of recombination. The quadrupole term on the other hand gets its contribution from the vorticity computed at the epoch of recombination (Eq. (4.15)). This, as we shall discuss below, is not the case for scalar and tensor anisotropies, as the dominant source of anisotropy is either constant (metric perturbations for tensor perturbations) or is increasing (compressional velocity mode for scalar perturbation) as the universe evolves. The third source of temperature anisotropies is metric vector perturbation V; this term can be comparable to the other terms only at super-horizon scales and hence we neglect this term in our analysis.

In Figure 4.1 we show the secondary temperature anisotropies generated during the epoch of reionization from vector modes. It is seen that the quadrupole term has significant contribution only for $\ell \lesssim 20$. The dominant contribution at larger ℓ is from the vorticity during reionization. The vorticity source contribution can be approximated as:

$$\frac{\Theta^{\rm v}_{T\ell}(\eta_0,k)}{(2\ell+1)} \simeq \frac{S(k)}{4\pi\rho_{\rm b0}}\frac{\eta_0^2}{\eta_{\rm reion}} j_\ell^{(11)}[k(\eta_0-\eta_{\rm reion})]\tau_{\rm reion} \tag{4.13}$$

for $\ell \leq 20$ and

$$\frac{\Theta^{\rm v}_{T\ell}(\eta_0,k)}{(2\ell+1)} \simeq \frac{S(k)}{k}\frac{1}{8\pi\rho_{\rm b0}}\frac{\eta_0^2 g(\eta_0-\ell/k,\eta_0)}{\eta_{\rm reion}}\sqrt{\frac{\pi}{\ell}} \tag{4.14}$$

for $\ell \gtrsim 50$. The temperature angular power spectrum from vorticity increases roughly as $\ell^{2.4}$ for $\ell \gtrsim 50$, with the signal reaching a value roughly $0.3\,\mu$k at $\ell \simeq 10^4$. This is in agreement with the results of Seshadri & Subramanian (2005).

4.3.2 Polarization anisotropies from vector modes

The main source of the polarization anisotropies is the temperature quadrupole $\Theta^{\rm v}_{T2}$. One contribution to the temperature quadrupole at the epoch of reionization is from the free-streaming of the dipole from the last scattering surface. The dipole at the last scattering surface can be obtained from the tight-coupling solutions to the temperature anisotropies (Mack et al. 2002). The quadrupole from the free-streaming of the dipole at the epoch of recombination is:

$$\Theta^{\rm v}_{T2}(\mathbf{k},\eta) = 5\Omega^{\rm v}_B(\mathbf{k},\eta_{\rm rec}) j_2^{(11)}(k(\eta-\eta_{\rm rec})) \tag{4.15}$$

Here $\eta_{\rm rec}$ corresponds to the epoch of recombination. As is the case for scalar perturbation-induced polarization in the reionized model (e.g. Zaldarriaga 1997) this quadrupole does not suffer the suppression as the quadrupole prior to the epoch of recombination when the

photons and baryons are tightly coupled. The structure of anisotropies generated by the quadrupole is determined by $j_2^{(11)}(k\eta)$ around the epoch of reionization. This typically gives a peak in anisotropies at $\ell \simeq 2\eta_0/\eta_{\rm reion}$. This source dominates the contribution to polarization anisotropies for $\ell \lesssim 10$. Another contribution to the temperature quadrupole at the epoch of reionization comes from the secondary temperature anisotropies generated at the epoch of reionization. The approximate value of this quadrupole can be got from retaining the first term in Eq. (4.4):

$$\frac{\Theta^{\rm v}_{T2}(\eta,k)}{(2\ell+1)} = \int_0^\eta d\eta'\, g(\eta,\eta')\Omega^{\rm v}_B(\eta')\, j_2^{(11)}[k(\eta-\eta')] \tag{4.16}$$

This contribution is generically smaller than the first contribution. Firstly, this depends on the vorticity evaluated close to the epoch of reionization as opposed to the first contribution which is proportional to the vorticity at the epoch of recombination. As the vorticity decays as $a^{-1/2}$ in the matter-dominated era (Eq. (4.12)), the latter contribution is suppressed by nearly a factor a 100 in the angular power spectrum. Second, as only a small fraction of photons re-scatter (nearly 20%), this contribution is further suppressed by a factor of $\tau^2_{\rm reion}$. However, this contribution is not suppressed at small angular scales and, therefore, might dominate the polarization anisotropies at large values of ℓ. In Figure 4.2, we show the E and B polarization angular power spectrum from the sources given by Eqs. (4.15) and (4.16). As discussed above, the secondary polarization anisotropies are dominated by the quadrupole generated by free-streaming of dipole at the last scattering surface. As expected for vector modes (Hu & White 1997), the B-mode signal is larger than the E-mode signal; the signal strength reaches $\simeq 10^{-3}\,\mu$k at $\ell \simeq 10$ in both cases. This dominates the primary signal for $\ell \lesssim 10$ as also seen in the numerical results of Lewis (2004). The contribution from the quadrupole generated at the epoch of reionization is seen to be completely sub-dominant.

4.4 CMBR anisotropies from tensor modes

The energy-momentum tensor for magnetic fields has a non-vanishing traceless, transverse component which sources the corresponding tensor metric perturbation. This in turn affects the propagation of radiation from the last scattering surface to the present and hence gets manifested as additional anisotropies. In this section we calculate the effect of reionization on the resultant anisotropies. For the temperature anisotropies, we study this effect, by calculating the power spectra separately for the standard recombination (no-reionization) and reionized scenario whereas for the polarization anisotropies we compute the secondary anisotropies by using the visibility function given by Eq (4.3).

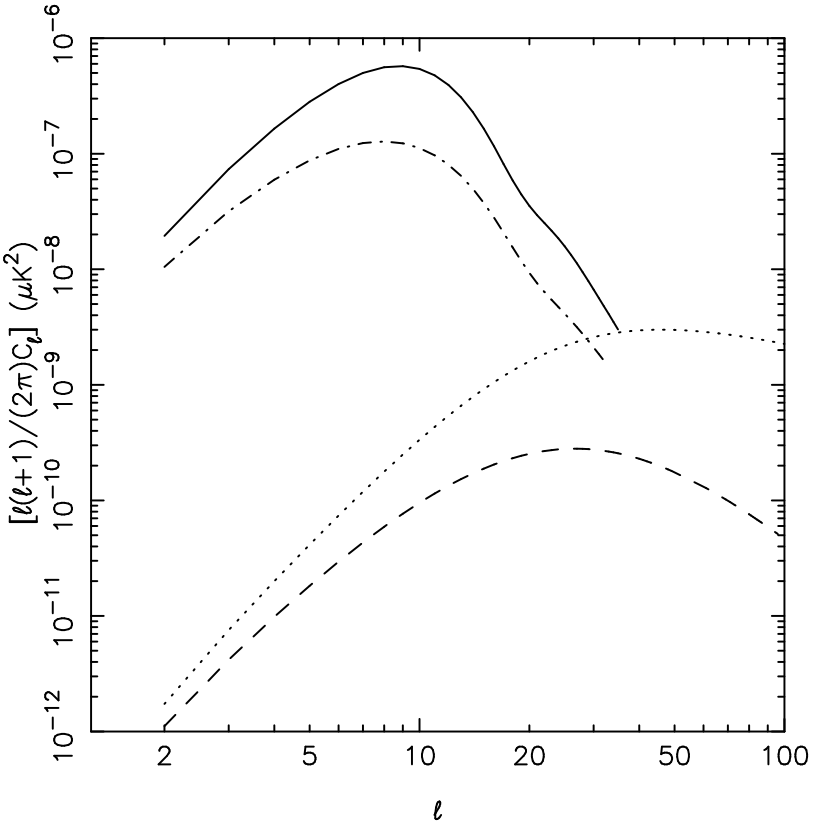

Figure 4.2: The secondary polarization angular power spectrum from vector modes is shown. The solid and the dot-dashed lines correspond, respectively, to the B and E mode contribution from the free-streaming quadrupole (Eq. (4.15)). The dotted and dashed curves B and E mode signals that arises from the source term given by Eq. (4.16). The power spectra are plotted for $B_0 = 3 \times 10^{-9}$ and $n = -2.9$ (Eq. (4.2)).

4.4.1 Tensor temperature anisotropies

The line-of-sight integral solution for temperature anisotropies, for tensor perturbations is given by (Hu & White 1997):

$$\frac{\Theta^T_{\ell T}(k,\eta_0)}{2\ell+1} = \int_0^{\eta_0} d\eta e^{-\tau}[\dot{\tau}P^{(T)} - \dot{h}]j_\ell^{(22)}[k(\eta_0-\eta)] \tag{4.17}$$

Here, $P^T(\eta) = 1/10[\Theta^{\rm T}_{T2} - \sqrt{6}\Theta^{\rm T}_{E2}]$ is the tensor polarization source and $\dot{h}$ is the gravitational wave contribution whose evolution is detailed in Appendix B. The polarization source is modulated by the visibility function and hence is localized to the last-scattering surface. In the tight coupling limit before recombination, $P^T \simeq -\dot{h}/(3\dot{\tau})$ (Mack et al. 2002). A more detailed derivation of P^T in the tight-coupling regime is given in Appendix B. In the post-recombination epoch, P^T is determined by the free-streaming of quadrupole generated at the last scattering surface. However, the visibility function is very small at epochs prior to reionization. Therefore the main contribution of this term comes only from epochs prior to recombination. The gravitational wave source on the other hand being modulated by the cumulative visibility $\exp(-\tau)$ contributes at all epochs. As a result, the P^T contributes negligibly to temperature anisotropies at all multipoles for the case of standard recombination. In the reionized model, this term gets additional contribution from epochs close to reionization redshift but continues to be sub-dominant to the other term. We have also checked this numerically. Hence we can neglect the first term in the above solution and using the matter-dominated solution for $\dot{h}$ (Appendix B), we arrive at the following expression for the angular power spectrum:

$$C^T_{\ell T} = \frac{4}{\pi}\left(\frac{9R_\gamma}{\rho_\gamma}\right)^2\left(\frac{8(l+2)!}{3(l-2)!}\right)\int dk k^2 \Pi^2_T(k)\left(\int_{x_d}^{x_0} dx \exp(-\tau)\frac{j_2(x)}{x}\frac{j_l(x_0-x)}{(x_0-x)^2}\right)^2 \tag{4.18}$$

Here, $x \equiv k\eta$, $x_0 \equiv k\eta_0$ and $x_d \equiv k\eta_{\rm rec}$. The above expression is evaluated numerically for the two different ionization histories: standard recombination with and without reionization which are essentially characterized by the different behaviour of the cumulative visibility $\exp(-\tau)$. The temperature power spectra are shown in Figure 4.3. As seen in the figure, the temperature power spectrum in both cases shows similar behaviour. The power is nearly flat upto $\ell \simeq 100$ after which the amplitude falls rapidly. This behaviour is identical to that obtained for primordial gravitational waves. This is expected because, the tensor metric perturbation is sourced by the magnetic field only upto the neutrino-decoupling epoch thereby imprinting an initial nearly scale-invariant spectrum after which the evolution is source-free. The effect of reionization is to reduce the cumulative visibility between recombination ($z \simeq 1100$) and reionization ($z \simeq 15$) epochs. Consequently, the signal is suppressed for the reionized model.

Approximate analytic expressions to primary $C_{\ell T}^T$ were derived in (Mack et al. 2002). However these give the correct qualitative behaviour $C_{\ell T}^T \propto \ell^{0.2}$ only for $\ell \lesssim 100$. This is because in their analytic results, the lower limit for the time-integral is taken to be zero in Eq. (4.18) whereas the correct lower limit is $\eta_{\rm rec}$ since the cumulative visibility is zero for $\eta \lesssim \eta_{\rm rec}$. We have not neglected this lower limit in our numerical calculation and hence we obtain the damping behaviour for $\ell \gtrsim 100$ as also observed in the numerical results of Lewis (2004). Our results are in reasonable agreement with the results of Lewis (2004) in the entire range of ℓ; these results also agree to within factors with the results of Mack et al. (2002) for $\ell \lesssim 75$ when the different convention we use for defining B_0 is taken into account. Our results are quantitatively accurate to better than 10% for the lower multipoles $\ell \lesssim 75$ but begin to differ appreciably from the results of numerical studies for larger ℓ or in the damping regime (Ng & Speliotopolous 1995). This is because we have not treated the transition regime from radiation-dominated to matter-dominated for the gravitational wave evolution accurately. As described in Appendix B, we have assumed instantaneous transition. This however does not affect the qualitative description of modes whose wavelength is greater than the transition-width $k \lesssim \eta_{\rm eq}^{-1}$ which in turn corresponds to multipoles $\ell \lesssim 300$.

4.4.2 Polarization anisotropies from tensor modes

The line-of-sight solution for the E and B-mode polarization is given as:

$$\frac{\Theta_{\ell B}^T(k,\eta_0)}{2l+1} = -\sqrt{6}\int_0^{\eta_0} d\eta \dot{\tau}\exp(-\tau)P^T\beta_l^T[k(\eta_0-\eta)] \tag{4.19}$$

$$\frac{\Theta_{\ell E}^T(k,\eta_0)}{2l+1} = -\sqrt{6}\int_0^{\eta_0} d\eta \dot{\tau}\exp(-\tau)P^T\epsilon_l^T[k(\eta_0-\eta)] \tag{4.20}$$

Here, β_l^T and ϵ_l^T are the tensor polarization radial functions as given in Hu & White (1997). The tensor polarization source $P^T(\eta)$ in this case will contribute significantly to the above integral only close to the reionization epoch. There are two contributions to the polarization at $\eta_{\rm reion}$: one due to the quadrupole generated at the reionization surface and the other due to the free-streaming primary quadrupole. However, as in the case of vector perturbations, the free-streaming primary quadrupole will give the dominant contribution. We thus have,

$$P^T(k,\eta) = \frac{1}{10}\Theta_{T2}^T(k,\eta) = -\frac{1}{2}\int_{\eta_{\rm rec}}^{\eta} d\eta \dot{h} j_2^{(22)}[k(\eta_0-\eta)]\exp(-\tau) \tag{4.21}$$

To simplify the calculations we make the following approximation. Since the visibility function is strongly peaked at $\eta_{\rm reion}$, we take P^T outside the integral by evaluating it at the visibility peak $\eta_{\rm reion}$. We have verified that this approximation works extremely well for the lower multipoles where the power is significant. We thus get the following expressions for

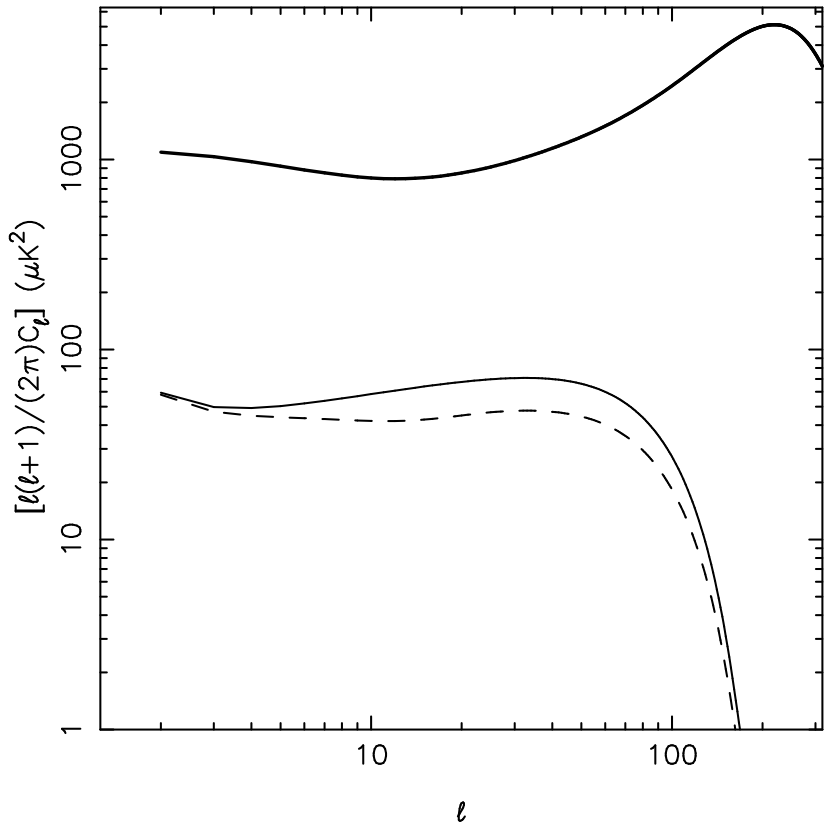

Figure 4.3: The contribution of tensor modes to the temperature power spectrum is shown. The solid and dashed lines give, respectively, the power spectra without and with reionization. The thick solid line, shown here for comparison, correspond to the temperature power spectrum from scalar modes, for the best-fit parameters from WMAP (Spergel 2003). The power spectra are plotted for $B_0 = 3 \times 10^{-9}$, $n = -2.9$ (Eq.(4.2)), and $\eta_\star/\eta_{\rm in} = 10^{18}$ (Eq. (4.43)).

the polarization angular power spectra:

$$C_{\ell B}^{T} = \frac{6}{\pi}\int dk k^2 \Pi_T^2(k)\left[P^T(\eta_{\rm reion})\right]^2\left(\int_{\eta_{\rm rec}}^{\eta_0} d\eta \dot{\tau} e^{-\tau}\beta_l^T[k(\eta_0-\eta)]\right)^2 \tag{4.22}$$

$$C_{\ell E}^{T} = \frac{6}{\pi}\int dk k^2 \Pi_T^2(k)\left[P^T(\eta_{\rm reion})\right]^2\left(\int_{\eta_{\rm rec}}^{\eta_0} d\eta \dot{\tau} e^{-\tau}\epsilon_l^T[k(\eta_0-\eta)]\right)^2 \tag{4.23}$$

As seen in the above expressions, the polarization power spectrum is modulated by the visibility function itself instead of the cumulative visibility in the case of temperature power spectrum. As a result, both E as well as B mode anisotropies peak close to the multipole corresponding to the horizon scale at reionization. Physically this can be understood as follows: the modes which are super-horizon at reionization experience negligible integrated Sachs-Wolfe effect before $\eta_{\rm reion}$ and hence very small polarization is generated for such modes. Maximum polarization is generated for modes that just enter the horizon at $\eta_{\rm reion}$. For sub-horizon modes, the amplitude of the gravitational wave falls and then sets itself into oscillations which is reflected as a drop in power for higher multipoles.

The polarization power spectra are shown in Figure 4.4. As seen in the figure, the E-mode power peaks at $\ell \sim 8$ whereas the B-mode power peaks at $\ell \sim 7$. The corresponding signal strengths at the peaks are $\sim 0.2\mu K$ in both cases. As expected, the E-mode power is marginally greater than the B-mode power mainly because of the slightly different behaviour of the radial projection factors (Hu & White 1997). The primary anisotropies for both the polarization modes is sub-dominant on these scales. This enhancement in the net (primary+secondary) signal was also seen in the numerical calculations of Lewis (2004).

We also show the primary CMBR polarization anisotropies from tensor modes in Figure 4.4. For computing these anisotropies we use the tight-coupling quadrupole, $P^T(\eta)$ as derived in Appendix B (Eq. (4.45)). The primary power spectra are also computed from Eqs. (4.22) and (4.23) with lower limit of the time integral replaced by zero. Our results are in agreement with the numerical results of Lewis (2004) when we take into account the fact that we use different value of $\eta_\star/\eta_{\rm in}$ (Eq. (4.43)): we use $\eta_\star/\eta_{\rm in} = 10^{18}$, which gives the epoch of generation of the tangled magnetic field close to inflationary epoch. While presenting numerical results, Lewis (2004) use $\eta_\star/\eta_{\rm in} = 10^6$, which puts the epoch of generation of magnetic field close to the epoch of electro-weak phase transition. Therefore our signal is roughly an order of magnitude larger than the results of Lewis (2004).

In Figure 4.5 we show the expected TE cross-correlation from tensor modes, computed using Eqs. (4.17), (4.20), and (4.21), including the effect of reionization. The effect of reionization is seen as the peak in the TE cross-correlation for $\ell \lesssim 10$. The signal is dominated by the primary signal for large multipoles. Note that the TE cross-correlation is positive in the entire range $\ell \lesssim 150$ as was also pointed out by Mack et al. (2002) for the primary tensor

TE cross-correlation (for details of sign of TE cross-correlation for various modes see (Hu & White 1997)). In the next section we compare this signal with the WMAP observation of TE cross-correlation.

4.5 Secondary CMBR anisotropies from scalar modes

In addition to the vortical component of the velocity field, the tangled magnetic fields also generate compressional velocity fields which seed density perturbations. These density perturbations have interesting consequences for the formation of structures in the universe (Wasserman 1978, Kim, Olinto & Rosner 1996, Subramanian & Barrow 1998, Sethi 2003, Gopal & Sethi 2003, Sethi & Subramanian 2005). The compressional velocity field also give rise to secondary anisotropies during the epoch of reionization. We compute this anisotropy here. The line-of-sight solution to the temperature anisotropies from these velocity perturbations is:

$$\frac{\Theta_\ell^S(k,\eta_0)}{2\ell+1} = \int_0^{\eta_0} d\eta e^{-\tau}\dot{\tau} v_{\rm b}^{\rm s}(k,\eta) j_\ell^{(10)}[k(\eta_0-\eta)] \tag{4.24}$$

Here $v_{\rm b}^{\rm s}$ is the line-of-sight component of the compressional velocity field. $j^{(10)}$ is defined in Hu & White (1997). The growing mode of compressional velocity can be expressed as (Wasserman 1978, Gopal & Sethi 2003):

$$v_{\rm b}^{\rm s}(\mathbf{k},\eta) = \frac{\eta}{4\pi\rho_{m0}}\hat{k}.\left(\text{F.T.}[\tilde{\mathbf{B}}(\mathbf{x})\text{x}(\nabla\text{x}\tilde{\mathbf{B}}(\mathbf{x}))]\right) \equiv v_{\rm b}^0(\mathbf{k})\eta \tag{4.25}$$

Here ρ_{m0} is the matter density (baryons and the cold dark matter) at the present epoch. The compressional velocity field, unlike the vortical mode, has a growing mode. Also unlike the vortical mode (Eq. (4.12)), the compressional mode of baryonic velocity couples to the dark matter (Gopal & Sethi 2003, Sethi & Subramanian 2005). In Figure 4.6 we show the angular power spectrum of the secondary temperature anisotropies generated by the compressional velocity mode. The signal has a peak at roughly the angular scale that corresponds to the width of the visibility function during reionization (for detailed discussion see e.g. Dodelson & Jubas 1994). The amplitude of this secondary anisotropy is several orders of magnitude smaller than the observed temperature anisotropies and it is unlikely that this signal could be detected.

4.6 Detectability

It follows from Figure 4.1 to 4.5, that the most important signal at small multipoles arises from tensor polarization anisotropies. In particular, the yet-undetected *B*-mode signal holds the promise of unravelling the presence of primordial magnetic fields, as also noted by other

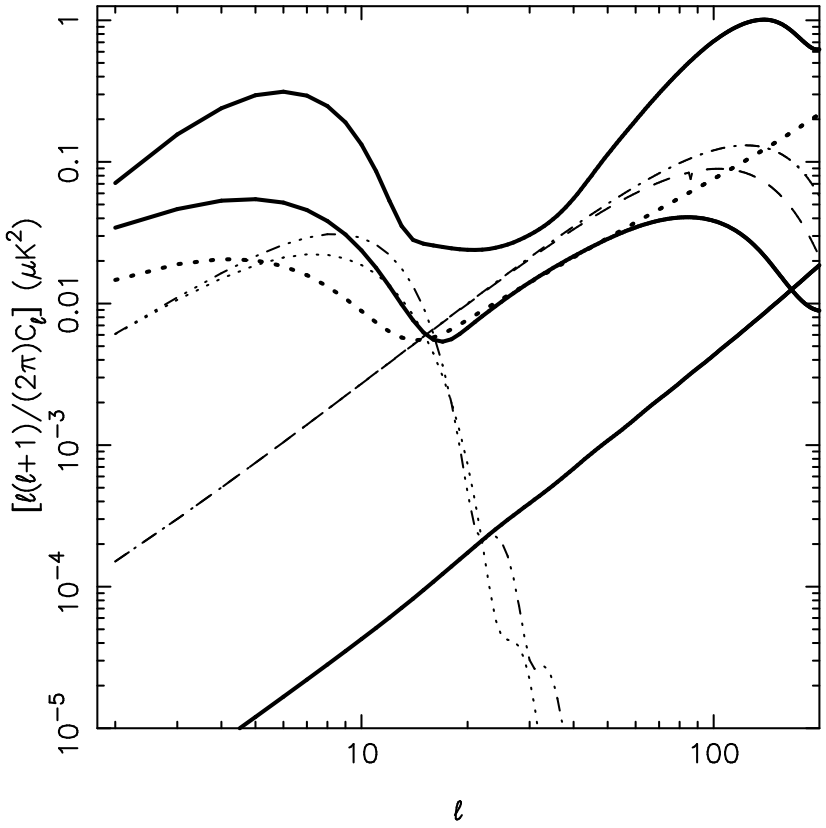

Figure 4.4: The tensor secondary and primary polarization power spectra are shown along with the expected signals from primordial scalar and tensor modes. The dot-dot-dot dashed and thin dotted lines correspond to the secondary E and B mode power spectra, respectively. The dot-dashed and dashed lines give the primary E and B mode power spectra. The two top solid lines, shown here for comparison, correspond to the E and B mode power spectra from primordial scalar modes, for the best-fit parameters from WMAP (Spergel 2003). For B mode signal we assume the ratio of tensor to scalar quadrupole $T/S = 0.7$ and the tensor spectral index $n_t = 0$. The bottom solid lines shows the B-mode signal expected from gravitational lensing. The thick dashed line shows the 1-σ errors expected from the future CMBR experiment Planck surveyor for one year of integration (Eq. (4.26)). The power spectra are plotted for $B_0 = 3 \times 10^{-9}$, $n = -2.9$ (Eq.(4.2)), and $\eta_\star/\eta_{\rm in} = 10^{18}$ (Eq. (4.43)).

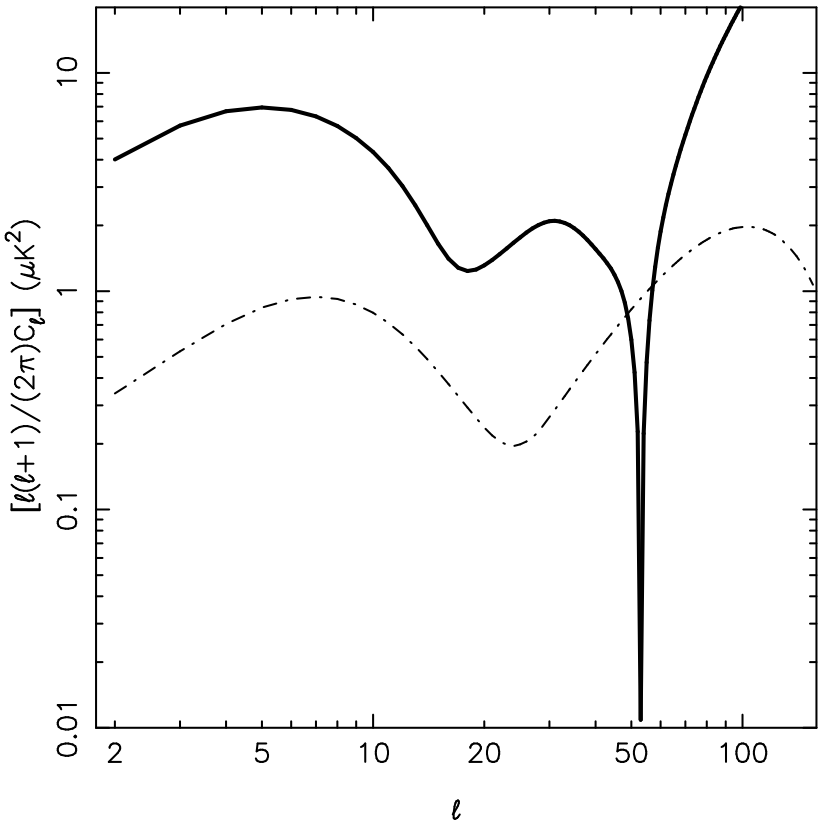

Figure 4.5: The tensor TE cross-correlation power spectra are shown along with the expected signal from primordial scalar modes. The dot-dashed shows the TE cross-correlation (secondary plus primary) from tangled magnetic fields. The thick solid line, shown here for comparison, correspond to the (absolute value of) TE cross-correlation power spectrum from primordial scalar modes, for the best-fit parameters from WMAP (Spergel 2003). The power spectrum is plotted for $B_0 = 3 \times 10^{-9}$, $n = -2.9$ (Eq.(4.2)), and $\eta_\star/\eta_{\rm in} = 10^{18}$ (Eq. (4.43)).

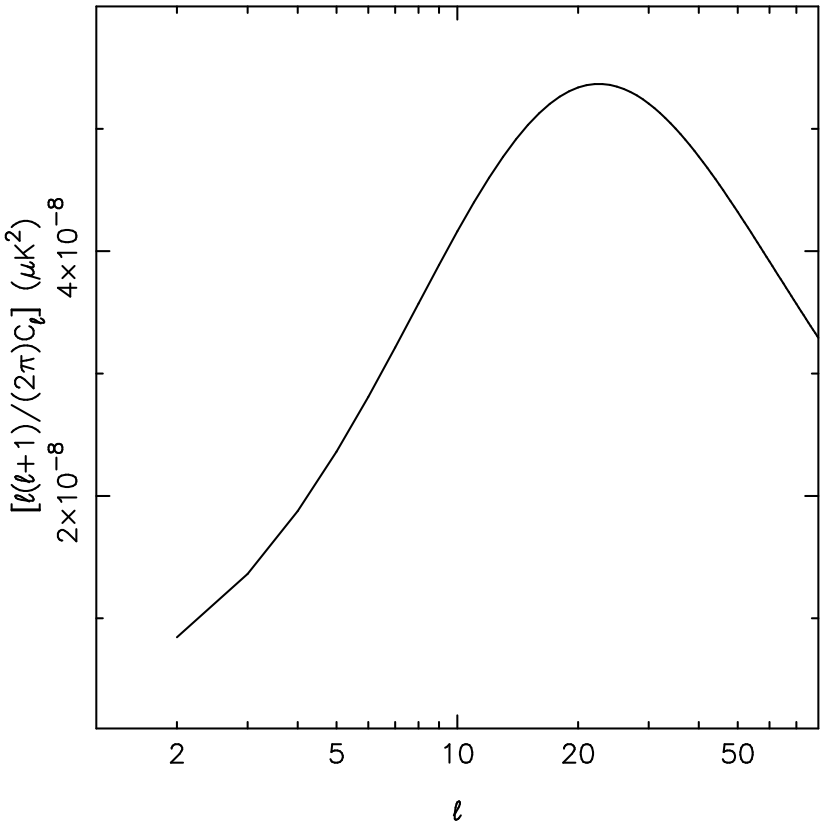

Figure 4.6: The secondary temperature power spectrum from scalar mode perturbations, seeded by tangled magnetic fields, is shown. The power spectrum is plotted for $B_0 = 3\times10^{-9}$ and $n = -2.9$ (Eq.(4.2)).

authors (e.g. (Lewis 2004)) In Figure 4.4, we show the expected errors on the detection of polarization signal from the future CMBR mission, Planck surveyor. The expected 1σ error, valid for $\ell \lesssim 100$, is (e.g. Zaldarriaga et al. (1997), Prunet, Sethi & Bouchet (2000)):

$$\Delta C_\ell = \left(\frac{2}{(2\ell+1) f_{\rm sky}}\right)\left(C_\ell + w^{-1}\right) \tag{4.26}$$

For Planck surveyor, $f_{\rm sky} \simeq 1$ and $w \simeq 1.7 \times 10^{16}$ for one-year integration. In Figure 4.4, we use the primordial tensor B-mode signal for calculating the expected 1σ error from Eq. (4.26). Figure 4.4 shows that the signal from magnetic fields with strength $\gtrsim 3\times10^{-9}$ G is detectable by this future mission. However, it is likely that, except for the B mode signal, the magnetic field signal will be buried in a larger signal. However, owing to the non-Gaussianity of the magnetic field signal it might still be possible to extract this component of the signal (e.g. (Lewis 2004)).

In Figure 4.5 we show the TE cross-correlation signal from tensor modes along with the expected signal from primordial scalar modes with $\tau_{\rm reion} = 0.17$, which is in good agreement with the WMAP data of TE cross-correlation (Kogut et al. 2003). It could be asked if the TE cross-correlation observed by WMAP for $\ell \lesssim 100$ could be explained as the tensor signal. From Figure 4.5 it is seen that the tensor signal at small multipoles is roughly a factor of 5 smaller than the scalar signal. And, therefore, as the power spectrum from tangled magnetic fields $\propto B_0^4$, much of the enhancement observed in the TE cross-correlation for $\ell \lesssim 10$ could be explainable in terms of the tensor signal from primordial magnetic field for $B_0 \simeq 4.5 \times 10^{-9}$ G. We quantify this notion by computing the χ^2 for $\ell \leq 15$ for both the best fit model from WMAP and the tensor model with $B_0 \simeq 4.5 \times 10^{-9}$ G against the detected WMAP signal [1] (Kogut et al. 2003); the χ^2 per degree of freedom in the two cases is $\simeq 1.7$ and $\simeq 1.8$, respectively. Therefore the enhancement can entirely be interpreted in terms of the secondary signal from primordial magnetic fields.

A more realistic possibility is that both primordial scalar and tensor modes gave comparable contribution to the observed signal. As the strength of both these signals for $\ell \lesssim 15$ is roughly $\propto \tau_{\rm reion}^2$ (for details of secondary scalar signal see e.g. Zaldarriaga 1997), and assuming that there is roughly equal contribution from both, the inferred value of $\tau_{\rm reion}$ from the analysis of the signal could be smaller by a factor of $\sqrt{2}$. To quantify this statement, we did a χ^2 test to estimate $\tau_{\rm reion}$ by adding the tensor signal with $B_0 \simeq 4.5\times10^{-9}$ G and the primordial scalar signal with the best-fit cosmological parameters from WMAP. From this analysis we obtain $\tau_{\rm reion} \simeq 0.11 \pm 0.02$ (1σ) with σ determined by $\delta\chi^2 = 1$. A possible test of this hypothesis is non-gaussianity of the signal at small multipoles, as the magnetic-field-sourced tensor signal is not Gaussian.

[1] for details of WMAP data products `http://map.gsfc.nasa.gov`

The tensor signal (primary plus secondary) could be appreciable for $\ell \lesssim 100$. In the range $15 \lesssim \ell \lesssim 100$, the tensor and primordial scalar signals are nearly independent of the value of $\tau_{\rm reion}$. While the primordial scalar TE signal anti-correlates for $\ell \gtrsim 40$, the tensor signal shows positive cross-correlation in the range $\ell \lesssim 100$, as seen in Figure 4.5. The present WMAP data shows tentative detection of TE anti-correlation for $\ell \lesssim 100$ (Peiris et al. 2003). From χ^2 analysis in the range $15 \lesssim \ell \lesssim 100$, we notice that the tensor signal alone is a poor fit to the data (χ^2 per degree of freedom of $\simeq 2.1$ as opposed to a value of 1.6 for the primordial scalar model). However a sum of these two signals with $B_0 \simeq 4.5 \times 10^{-9}\,{\rm G}$ is a reasonable fit, as it is dominated by the primordial scalar signal.

It should be noted that for $B_0 \simeq 4.5 \times 10^{-9}\,{\rm G}$, the tensor temperature signal is comparable to the primordial scalar signal (Figure 4.3). WMAP analysis obtained an upper limit of $\simeq 0.7$ on the ratio of tensor to scalar signal (Spergel 2003). While this limit is rather weak, a more detailed analysis of the temperature signal including the effect of tensor mode signal sourced by primordial magnetic fields might give independent constraints on the strength of primordial magnetic fields.

In our χ^2 analysis we use only the diagonal components of the Fisher matrix. However, owing to incomplete sky, the signal is correlated, especially for small multipoles, across neighboring multipoles. However, a more comprehensive analysis taking into this correlation is likely to yield similar conclusions for the reasons stated above.

Our conclusions are not too sensitive to the value of small scale cut-off $k_{\rm max}$ or the scale of the filter k_c used to define the normalization (Eq. (4.2)) for magnetic field power spectrum index $n = -2.9$ we use throughout the chapter. For $k_{\rm max} = k_c = 0.05\,{\rm Mpc}^{-1}$, the foregoing discussion related to tensor mode anisotropies would be valid for $B_0 \simeq 5 \times 10^{-9}\,{\rm G}$. Therefore, the results for TE cross-correlation from tensor perturbations can be interpreted to put bounds on magnetic fields for only large scales $k \lesssim 0.05\,{\rm Mpc}^{-1}$.

The strongest bound on primordial magnetic fields arises from tensor perturbations in the pre-recombination era (Caprini & Durrer 2001). These bounds are weakest for nearly scale invariant ($n \simeq -3$) magnetic fields power spectrum (Eq. (33) of Caprini & Durrer 2001) and largely motivated the choice of the power spectral index we consider here. For $n = -2.9$, the bound obtained by Caprini & Durrer (2001) is considerably weaker than $B_0 \simeq 4.5 \times 10^{-9}\,{\rm G}$, the values of interest to us in this chapter. Vector modes might leave observable signature in the temperature and polarization signal for $\ell \gtrsim 2000$; the current observations give weak bound of $B_0 \lesssim 8 \times 10^{-9}\,{\rm G}$ (Lewis 2004). Tangled magnetic-field-sourced primary scalar temperature signal gives even weaker bounds Koh & Lee (2000). More recently, (Chen et al. 2004) obtained, from WMAP data analysis, a limit of $\lesssim 10^{-8}\,{\rm G}$ on the primordial magnetic field strength for nearly scale invariant spectra we consider here; (Chen et al. 2004) consider vector mode temperature signal in their analysis and study possible non-Gaussianity

in the WMAP data. Another strong constraint on large scale tangled magnetic fields comes from Faraday rotation of high redshift radio sources (see e.g Widrow 2002); this constraint is also weaker than the value of magnetic field required to explain the enhancement of the TE cross-correlation signal as seen by WMAP (Sethi 2003). Therefore, the value of B_0 required to give appreciable contribution to the TE signal is well within the upper limits on B_0 from other considerations.

It should be noted that the entire foregoing discussion on the tangled-magnetic-field tensor signal can be mapped to primordial tensor modes. The reason for this assertion is that magnetic fields source tensor modes only prior to the epoch of neutrino decoupling, and the subsequent evolution is source free, which is similar to the primordial tensor modes which are generated only during the inflationary epoch and evolve without sources at subsequent times. Therefore, an analysis similar to ours could be used to put constraints on the relative strength of the tensor to scalar mode contribution (for a fixed scale) and the tensor spectral index of the primordial modes. The main observational difference between such an interpretation and the one give here is that tensor signal sourced by magnetic fields will not obey Gaussian statistics as opposed to the primordial tensor modes.

4.7 Summary and conclusions

We have computed the secondary anisotropies from the reionization of the universe in the presence of tangled primordial magnetic fields. Throughout our analysis we use the nearly scale invariant magnetic field power spectrum with $n = -2.9$. For vector modes, we compute the secondary temperature and E and B mode polarization auto-correlation signal. For scalar modes, the results for secondary temperature angular power spectrum from compressional velocity modes are presented. For tensor modes, in addition to the secondary temperature and polarization angular power spectra, we compute the TE cross-correlation signal and compare it with the existing WMAP data; we also recompute the primary signal for tensor modes. Whenever possible we compare our results with the results existing in the literature. In particular, (Lewis 2004) recently computed fully-numerically the vector and tensor primary and secondary temperature and polarization power spectra. We compare our semi-analytic results with this analysis and find good agreement. Seshadri & Subramanian (2005) computed the secondary temperature anisotropies from vector modes. Our results are in good agreement with their conclusion. Mack et al. (2002) computed primary signal from vector and tensor modes using the formalism we adopt in this chapter. Our results are in disagreement with their results for $\ell \gtrsim 75$, and we have given reasons for our disagreement in the discussion above. In addition to comparison with existing literature, we also give new results for secondary TE cross-correlation from tensor modes and secondary temperature

angular power spectrum from scalar modes.

We discuss below the details of expected signal from each of the perturbation mode: *Vector modes*: The secondary temperature and polarization signals from the vector modes is shown are Figure 4.1 and 4.2. The secondary temperature signal increases $\propto \ell^{2.4}$ for $\ell \gtrsim 50$ and reaches a value $\simeq 0.1\,(\mu\mathrm{k})^2$ for $\ell \simeq 10^4$, in agreement with the analysis of Seshadri & Subramanian (2005). For small ℓ the signal is very small ($\lesssim 10^{-4}\,(\mu\mathrm{k})^2$) and for large ℓ the secondary signal is smaller than the primary signal (e.g. (Lewis 2004)) and therefore it is unlikely that the signature of reionization could be detected in the vector-mode temperature anisotropies. The polarization signal, shown in Figure 4.2, is sourced by the free-streaming of dipole at the epoch of recombination. This signal dominates the primary signal for $\ell \lesssim 10$, but is several orders of magnitude smaller than the expected signal from tensor modes.

Scalar modes: We only compute the secondary temperature anisotropies from compressional velocity modes in this case. As seen in Figure 4.6, this contribution is several orders of magnitude smaller than the already-detected primary signal and therefore its effects are unlikely to be detectable.

Tensor modes: As seen from Figures 4.4 and 4.5, the most interesting CMBR anisotropy signal for $\ell \lesssim 100$ is from these modes. The secondary B-mode signal from tensor modes is detectable by future CMBR mission Planck surveyor for $B_0 \simeq 3 \times 10^{-9}\,\mathrm{G}$. The tensor TE cross correlation from primordial magnetic fields can explain the observed enhancement of the observed signal for $\ell \lesssim 10$ by WMAP for $B_0 \simeq 4.5 \times 10^{-9}\,\mathrm{G}$ if the primordial magnetic fields are generated during the epoch of inflation. Assuming that tensor modes make a significant contribution to the observed enhancement, the bounds on the optical depth to the surface of reionization, τ_{reion} are weaker by roughly a factor of $\sqrt{2}$. This hypothesis can be borne/ruled out by testing the Gaussianity of the signal for $\ell \lesssim 10$

Appendix A

In this section, we briefly discuss the terminology and present the complete expressions for the vector and tensor power spectra $\Pi^V(k)$ and $\Pi^T(k)$ (Mack et al. 2002). The energy momentum tensor for magnetic fields for a single Fourier mode is a convolution of different Fourier modes and is given by:

$$T_{ij}(\mathbf{k}) = \int d^3q \left[\tilde{B}_i(\mathbf{q})\tilde{B}_j(\mathbf{k}-\mathbf{q}) - \frac{1}{2}\delta_{ij}\tilde{B}_m(\mathbf{q})\tilde{B}_m(\mathbf{k}-\mathbf{q}) \right] \tag{4.27}$$

The energy-momentum tensor has non-vanishing scalar, vector, and tensor components. The vector and tensor components, in Fourier space, are defined as:

$$\Pi_i^V = P_{ip}\hat{k}_q T_{pq} \tag{4.28}$$

$$\Pi^T_{ij} = \left(P_{ip}P_{jq} - \frac{1}{2}P_{ij}P_{pq} \right) T_{pq} \tag{4.29}$$

Here $P_{ij} = \delta_{ij} - \hat{k}_i\hat{k}_j$. The vector and tensor anisotropic stress are then defined as the two-point correlations of the above components as:

$$\langle \Pi^V_i(\mathbf{k})\Pi^V_i(\mathbf{k}')\rangle \equiv 2|\Pi^{(V)}(k)|^2\delta(\mathbf{k}+\mathbf{k}') \tag{4.30}$$

$$\langle \Pi^T_{ij}(\mathbf{k})\Pi^T_{ij}(\mathbf{k}')\rangle \equiv 4|\Pi^{(T)}(k)|^2\delta(\mathbf{k}+\mathbf{k}') \tag{4.31}$$

By evaluating the above correlations as also given in Mack et al. (2002), we can arrive at the following approximate expression for the power spectra for $n < -3/2$.

$$|\Pi_V(k)|^2 = \frac{A^2}{64\pi^4(n+3)}k^{2n+3} \tag{4.32}$$

$$|\Pi_T(k)|^2 = \frac{2A^2}{64\pi^4(n+3)}k^{2n+3} \tag{4.33}$$

Here, A is the normalization of the magnetic power spectrum given in Eq. (4.2)

Appendix B

Gravitational waves correspond to transverse,traceless perturbations to the metric: $\delta g_{ij} = 2a^2(\eta)h_{ij}$ with $h_{ii} = \hat{k}_i h_{ij} = 0$. Since h_{ij} is a stochastic variable we can define its power spectrum as:

$$\langle h_{ij}(\mathbf{k},\eta)h_{ij}(\mathbf{k}',\eta)\rangle = 4|h(k,\eta)|^2\delta(\mathbf{k}+\mathbf{k}') \tag{4.34}$$

The evolution of h_{ij} then follows from the tensor Einstein equation (see e.g. Hu & White 1997) ,

$$\ddot{h} + 2\frac{\dot{a}}{a}\dot{h} + k^2 h = 8\pi G S(k,\eta) \tag{4.35}$$

The source on the RHS is the tensor anisotropic stress of the plasma which is defined as: $S(k,\eta) = \Pi^T(k)/a^2$ (Eq. (4.31)). We assume that the primordial magnetic fields are generated by some mechanism at a very early epoch η_{in}. It was recently shown by Lewis (2004) that after the neutrino decoupling epoch $\eta_\star$ the neutrino start free-streaming and develop significant anisotropic stress which cancel the anisotropic stress of the primordial magnetic fields to the leading order for super-horizon modes, resulting in negligible net anisotropic stress in the plasma. We can thus assume that for $\eta \gg \eta_\star$, $S(\mathbf{k},\eta) = 0$ and for $\eta \ll \eta_\star$, $S(\mathbf{k},\eta) = \Pi^T(k)/a^2$ where $\Pi^T(k)$ is the magnetic tensor anisotropic stress as defined in Eq. (4.31). We now derive the solutions to Eq. (4.35) in various regimes. The evolution of the scale factor $a(\eta)$ is given by the Friedmann equation:

$$\dot{a}^2 = H_0^2(\Omega_m a + \Omega_\gamma + \Omega_\nu + \Omega_\Lambda a^4) \tag{4.36}$$

Here, $\Omega_{m,\gamma,\nu,\Lambda}$ are the fractional densities in matter, radiation,neutrinos and cosmological constant respectively. Approximate solutions in the radiation-dominated and matter-dominated epoch are $a(\eta) = 2\sqrt{\frac{\Omega_\gamma+\Omega_\nu}{\Omega_m}}\frac{\eta}{\eta_0}$ and $a(\eta) = \left(\frac{\eta}{\eta_0}\right)^2$ respectively. Using the above form for the scale-factor we can rewrite Eq. (4.35) for $\eta_{in} < \eta < \eta_\star$ as:

$$\ddot{h} + \frac{2}{\eta}\dot{h} + k^2 h = \frac{3R_\gamma \Pi^T(k)}{\rho_\gamma}\frac{1}{\eta^2} \tag{4.37}$$

Here, $R_\gamma = \Omega_\gamma/(\Omega_\gamma + \Omega_\nu) \simeq 0.6$. ρ_γ is the CMBR energy density. Eq. (4.37) can be solved exactly using the Green's function technique to give (Mack et al. 2002):

$$h(k,\eta) = \frac{3R_\gamma \Pi^T(k)}{\rho_\gamma}\int_{\eta_{in}}^{\eta} d\eta^{'}\frac{\sin[k(\eta-\eta^{'})]}{\eta^{'}} \tag{4.38}$$

For super-horizon modes $k\eta \ll 1$, the above form can be simplified to give:

$$h(k,\eta) \approx \frac{3R_\gamma \Pi^T(k)}{\rho_\gamma}\int_{\eta_{in}}^{\eta} d\eta^{'}\frac{k(\eta-\eta^{'})}{k\eta\eta^{'}} = \frac{3R_\gamma \Pi^T(k)}{\rho_\gamma}\ln\left(\frac{\eta}{\eta_{\rm in}}\right) \tag{4.39}$$

For $\eta \gg \eta_\star$, the evolution of h is given by the homogeneous solutions in the radiation and matter-dominated regimes:

$$h_{rad}(k,\eta) = A_1 j_0(k\eta) \tag{4.40}$$

$$h_{mat}(k,\eta) = A_2\frac{j_1(k\eta)}{k\eta} \tag{4.41}$$

The coefficients A_1 and A_2 are determined by matching the super-horizon solutions at the two transitions $\eta_\star$ and η_{eq}. We thus get

$$A_2 = 3A_1 = \frac{9R_\gamma \Pi^T(k)}{\rho_\gamma}\ln\left(\frac{\eta_\star}{\eta_{\rm in}}\right) \tag{4.42}$$

Thus, the full expression for the matter-dominated solution can be written as:

$$\dot{h}_{mat}(\eta,k) = \frac{9R_\gamma \Pi^T(k)}{\rho_\gamma}\ln\left(\frac{\eta_\star}{\eta_{\rm in}}\right)\frac{j_2(k\eta)}{\eta} \tag{4.43}$$

This solution is used for solving tensor temperature and polarization primary and secondary anisotropies. Few assumptions have been made in deriving the above expression. Firstly, the transition between radiation dominated to matter-dominated region has been assumed to be instantaneous. This however does not affect the evolution of modes with wave-length greater than the width of transition $k\eta_{\rm eq} \lesssim 1$. Moreover, only super-horizon solutions have been used to match the solutions for h at different transitions. These simplifications however do not affect the results quotes for small multipoles as discussed in the main section.

Tight-coupling tensor quadrupole

In the tight-coupling regime, $z \gtrsim 1100$, to lowest order in mean-free path, we have $P^T = -\dot{h}/(3\dot{\tau})$ (Mack et al. 2002). We however use the expression accurate to the second order in mean-free path as is done for the scalar modes in Zaldarriaga & Hariri (1995). Using the Boltzmann equation for the evolution of tensor modes we get the following equation for $P^T(\mathbf{k}, \eta)$ in the tight-coupling limit:

$$\dot{P} + \frac{3}{10}\dot{\tau}P = -\frac{\dot{h}}{10} \tag{4.44}$$

The lowest order solution to this equation is obtained by neglecting the $\dot{P}$ in the equation, which gives, $P = -\dot{h}/(3\dot{\tau})$. The above equation however can be solved exactly to give:

$$P(\eta) = \int_0^\eta d\eta' \dot{h} e^{-\frac{3}{10}[\tau(\eta') - \tau(\eta)]} \tag{4.45}$$

We use the standard recombination history for computing τ.

Bibliography

Barrow J.D., Ferreira P.G., & Silk J., 1997, Phys. Rev. Lett., 78, 3610

Caprini C. & Durrer R., Phys. Rev. D., 2001, 65, 023517

Chen G., Mukherjee P., Kahniashvili T., Ratra B. & Wang Y., ApJ, 2004, 611, 655

Dodelson S. & Jubas J.M., ApJ, 1994, 439, 503

Durrer R., Ferreira P.G., Kahniashvili T., 2000, Phys. Rev. D., 61, 043001

Freedman W.L. et al. , ApJ, 2001, 553, 47

Giovannini M., 2005, astro-ph/0508544

Gopal R. & Sethi S.K., 2003, Journal of Astrophysics & Astronomy, 24, 51

Hu W. & Dodelson S., ARA&A, 2002, 40, 171

Hu W. & White M., Phys. Rev. D., 1997, 56, 596

Jedamzik K., Kataliniċ V. & Olinto A.V., Phys. Rev. D., 1998, 57, 3264

Kim, E.-J., Olinto A.V., Rosner R., 1996, ApJ 468, 28

Kogut A. et al. , ApJS, 2003, 148, 161

Koh S. & Lee C.H., Phys. Rev. D., 2000, 62, 083509

Kovac J.M., Leitch E.M., Pryke C., Carlstrom J.E., Halverson N.W. & Holzapfel W.L., Nature, 2002, 420, 772

Landau L.D. & Lifshitz E.M., Fluid Mechanics, 1987, Pergamon Press

Lewis A., Phys. Rev. D., 2004, 70, 43011

Mack A., Kahniashvili T. & Kosowsky A., 2002, Phys. Rev. D., 65, 123004

Ng K.W. & Speliotopolous A.D., Phys. Rev. D., 1995, 52, 2112

Peiris H.V. et al. , ApJS, 2003, 148, 213 (2003)

Perlmutter S. et al. , ApJ, 1999, 517, 565

Prunet S., Sethi S.K. & Bouchet F., MNRAS, 2000, 314, 348

Ratra B., 1992, ApJ Lett., 391, L1

Riess A.G. et al. , ApJ, 2004, 607, 665

Ruzmaikin A.A., Shukurov A.M., Sokoloff D.D., *Magnetic Fields of Galaxies*, Kluwer, Dordrecht (1988) Kluwer Acad. Publ., Dordrecht. (2004)

Seshadri T.R. & Subramanian K., Phys. Rev. D., 2005, 72, 023004

Seshadri T.R. & Subramanian K., 2001, Phys. Rev. Lett., 87, 101301

Sethi S.K. & Subramanian K., MNRAS, 2005, 356, 778

Sethi S.K., 2003, MNRAS, 342, 962

Shukurov A., 2004, Introduction to galactic dynamos, In Mathematical aspects of natural dynamos, Ed. E. Dormy, Kluwer Acad. Publ., Dordrecht.

Spergel D.N., ApJS, 2003, 148, 175

Subramanian K. & Barrow J.D., 2002, MNRAS, 335, L57

Subramanian K. & Barrow J.D., 1998, Phys. Rev. D., 58, 83502

Subramanian K. & Barrow J. D., 1998, Phys. Rev. Lett., 81, 3575

Tegmark M. et al. , Phys. Rev. D., 2004, 69, 103501

Tytler D., O'Meara J.M., Suzuki N. & Lubin D., Physics Reports, 2000, 333, 409

Wasserman I., 1978, ApJ, 224, 337

Widrow L.M., Rev. Mod. Phys., 74, 775

Zaldarriaga M., Phys. Rev. D., 1997, 55, 1822

Zaldarriaga M., Spergel D.N. & Seljak U., ApJ, 1997, 488, 1

Zaldarriaga M. & Hariri D.D., Phys. Rev. D., 1995, 52, 3276